


REPORT

# Regulation of ETAA1-mediated ATR activation couples DNA replication fidelity and genome stability

Divya Achuthankutty<sup>1,2\*</sup>, Roshan Singh Thakur<sup>2\*</sup> , Peter Haahr<sup>1\*</sup> , Saskia Hoffmann<sup>1</sup>, Alexandros P. Drinas<sup>3</sup>, Anna H. Bizard<sup>2</sup>, Joachim Weischenfeldt<sup>4</sup>, Ian D. Hickson<sup>2</sup>, and Niels Mailand<sup>1,2</sup> 

The ATR kinase is a master regulator of the cellular response to DNA replication stress. Activation of ATR relies on dual pathways involving the TopBP1 and ETAA1 proteins, both of which harbor ATR-activating domains (AADs). However, the exact contribution of the recently discovered ETAA1 pathway to ATR signaling in different contexts remains poorly understood. Here, using an unbiased CRISPR-Cas9-based genome-scale screen, we show that the ATR-stimulating function of ETAA1 becomes indispensable for cell fitness and chromosome stability when the fidelity of DNA replication is compromised. We demonstrate that the ATR-activating potential of ETAA1 is controlled by cell cycle- and replication stress-dependent phosphorylation of highly conserved residues within its AAD, and that the stimulatory impact of these modifications is required for the ability of ETAA1 to prevent mitotic chromosome abnormalities following replicative stress. Our findings suggest an important role of ETAA1 in protecting against genome instability arising from incompletely duplicated DNA via regulatory control of its ATR-stimulating potential.

## Introduction

The ATR kinase plays a crucial role in normal physiology by functioning as an apical organizer of the cellular response to DNA replication stress, a deleterious condition caused by the slowing or stalling of replication forks (Saldivar et al., 2017). Replication stress is a recognized driver of genome instability that can fuel the development of cancer and other severe pathologies (Branzei and Foiani, 2010; Ciccio and Elledge, 2010; Zeman and Cimprich, 2014). ATR-dependent phosphorylation of a range of downstream effector proteins collectively enables cells to prevent the collapse of stalled replication forks and suppress the firing of new replication origins until the replicative stress has been resolved (Saldivar et al., 2017).

Stimulation of ATR kinase activity entails the recruitment of ATR and its partner protein ATRIP to replication protein A (RPA)-coated stretches of single-stranded DNA, which accumulate upon functional uncoupling of replicative DNA helicase and polymerase activities after replication fork stalling (Zou and Elledge, 2003; Saldivar et al., 2017). This brings ATR-ATRIP into close proximity with TopBP1, which is independently recruited to replication stress sites via the Rad9-Rad1-Hus1 complex and

directly stimulates ATR kinase activity by means of an ATR-activating domain (AAD; Kumagai et al., 2006; Delacroix et al., 2007; Lee et al., 2007). While the requirement of this pathway for promoting the essential ATR–CHK1 checkpoint signaling axis has long been recognized, recent findings revealed that the ETAA1 protein independently promotes ATR signaling by means of dual RPA-binding motifs and an AAD that stimulates ATR kinase activity via a mechanism analogous to that of the TopBP1 AAD (Bass et al., 2016; Haahr et al., 2016; Lee et al., 2016; Thada and Cortez, 2019). Loss of ETAA1 sensitizes cells to replication stress and is synthetic lethal with TopBP1 depletion, resulting from quantitative suppression of ATR signaling, defective G2/M checkpoint control, and ensuing gross chromosomal instability (Haahr et al., 2016). Thus, full ATR activation in vertebrate cells relies on independent TopBP1- and ETAA1-mediated pathways, although the precise division of labor in promoting ATR-mediated signaling responses remains unclear. For instance, while ablation of TopBP1 or the functionality of its AAD leads to early embryonic lethality in mice, ETAA1 knockout (KO) gives rise to a comparatively mild phenotype characterized by

<sup>1</sup>Protein Signaling Program, Novo Nordisk Foundation Center for Protein Research, Copenhagen, Denmark; <sup>2</sup>Center for Chromosome Stability, Department of Cellular and Molecular Medicine, University of Copenhagen, Copenhagen, Denmark; <sup>3</sup>Department of Pediatrics and Genetics, Stanford University, Stanford, CA; <sup>4</sup>Biotech Research and Innovation Center, University of Copenhagen and Finsen Laboratory, Copenhagen, Denmark.

\*D. Achuthankutty, R.S. Thakur, and P. Haahr contributed equally to this paper; Correspondence to Ian D. Hickson: [iandh@sund.ku.dk](mailto:iandh@sund.ku.dk); Niels Mailand: [niels.mailand@cpr.ku.dk](mailto:niels.mailand@cpr.ku.dk).

© 2019 Achuthankutty et al. This article is distributed under the terms of an Attribution–Noncommercial–Share Alike–No Mirror Sites license for the first six months after the publication date (see <http://www.rupress.org/terms/>). After six months it is available under a Creative Commons License (Attribution–Noncommercial–Share Alike 4.0 International license, as described at <https://creativecommons.org/licenses/by-nc-sa/4.0/>).

incompletely penetrant embryonic lethality, reduced body size, and defective clonal expansion of T lymphocytes (Zhou et al., 2013; Miosge et al., 2017). Recent studies suggested roles of ETAA1 in promoting an ATR-mediated S/G2 checkpoint suppressing mitotic entry before completion of DNA replication and ATR activation during mitosis, where ATR has been shown to facilitate Aurora B activation at centromeres and accurate chromosome segregation (Kabeche et al., 2018; Saldivar et al., 2018; Bass and Cortez, 2019). However, it remains unclear which, if any, of these activities represents the key cellular functions of ETAA1 in maintaining chromosome stability. In addition, whether and how the ATR-activating capacity of ETAA1 is modulated by DNA replication and genome integrity status are not known.

Here, we used an unbiased genome-scale CRISPR-Cas9 screening approach to reveal a specific and critical function of ETAA1 in promoting cell fitness and chromosome stability upon genetic or chemical disruption of DNA replication efficiency. We established a central role in this process of cell cycle- and replication stress-regulated, phosphorylation-dependent control of ETAA1-mediated ATR activation.

## Results and discussion

### ETAA1 becomes critical for cell fitness upon disruption of the DNA replication machinery

To define the key cellular functions of human ETAA1, we performed an unbiased, genome-scale, CRISPR-Cas9-based screen to identify genes whose ablation is synthetic lethal with loss of ETAA1 expression. To this end, we transduced WT and ETAA1-deficient (*ETAA1Δ*) HeLa cells (Haahr et al., 2016) with a lentiviral CRISPR-Cas9 KO single guide RNA (sgRNA) library (GeCKO v2) targeting 19,050 human genes (Sanjana et al., 2014). We then used next-generation sequencing to identify sgRNAs that were selectively depleted in the *ETAA1Δ* background upon long-term proliferation (Fig. 1 A and Fig. S1 A). Among genes whose KO selectively impaired proliferation of *ETAA1Δ* cells, we identified several factors with known roles in promoting DNA synthesis, including MCM10, POLE3, POLE4, and CDC25A (Bartek et al., 2004; Chadha et al., 2016; Bellelli et al., 2018), while sgRNAs targeting essential DNA replication factors including proliferating cell nuclear antigen and CMG helicase subunits were depleted in both WT and *ETAA1Δ* cells as expected (Fig. 1, B and C; Fig. S1 B; and Table S1). Gene ontology analysis indicated notable enrichment of terms associated with DNA replication and cell cycle progression among gene KOs displaying synthetic lethality with ETAA1 loss (Fig. 1 D), suggesting that ETAA1 function becomes critical when DNA replication efficiency is compromised. Knockdown of MCM10 or POLE3 by siRNAs impaired clonogenic survival to a much greater extent in HCT116 *ETAA1Δ* cells than in their WT counterparts, validating these screen hits and demonstrating that their genetic interaction with ETAA1 is not cell type-specific (Fig. 1, E and F; and Fig. S1, C and D). Interestingly, combined loss of ETAA1 and MCM10 led to a markedly elevated proportion of cells undergoing mitosis in the presence of DNA damage relative to MCM10 depletion alone (Fig. 1, G and H). Moreover, upon low-dose treatment with the DNA polymerase

inhibitor aphidicolin (APH) to chemically slow down DNA replication, *ETAA1Δ* cells displayed a faster progression into mitosis than did WT cells (Fig. 1 I). Together, these data suggest that ETAA1 function becomes critical for cell fitness and genome stability by restraining mitotic entry when DNA replication integrity is compromised.

### ETAA1 prevents mitotic chromosome abnormalities associated with under-replicated DNA

To explore the potential role of ETAA1 in preventing genetic alterations arising from incompletely replicated DNA, we analyzed the impact of ETAA1 loss in HCT116 and HeLa cells on mitotic chromosome abnormalities. For this, we quantified bulky and ultrafine anaphase DNA bridges (UFBs) that are hallmarks of unresolved replication intermediates (Mankouri et al., 2013), during both an unperturbed cell cycle and following replication stress induced by low-dose treatment with APH or hydroxyurea (HU). Consistent with a role of ETAA1 in linking DNA replication integrity and chromosome stability, *ETAA1Δ* cells showed elevated frequencies of anaphase chromatin bridges and lagging chromatin that were exacerbated upon replicative stress (Fig. 2, A–C; and Fig. S1, E–H). Likewise, *ETAA1Δ* cells displayed a pronounced increase in UFBs marked by PICH and associated with FANCD2 twin foci (Fig. 2, A and D–F; and Fig. S1, I and J), indicative of elevated common fragile site (CFS) expression (Minocherhomji et al., 2015). In late G2 cells, ETAA1 colocalized with FANCD2 foci, which demarcate CFSs, but not with centromeric or telomeric markers (Fig. S1 K), suggesting a specific association of ETAA1 with UFBs arising from under-replicated DNA. We also observed a subset of UFBs that were coated by RPA (Fig. S1, L and M; Mankouri et al., 2013; Chan et al., 2018), although we failed to detect ETAA1 associated with these structures (data not shown), suggesting that it suppresses UFB formation by restricting mitotic entry of cells containing incompletely duplicated loci. In agreement with this possibility, cells lacking ETAA1 displayed an increased level of metaphase chromosome breaks that was further enhanced following APH treatment (Fig. 2, A, G, and H). Moreover, ETAA1 KO led to a markedly elevated proportion of APH-treated and MCM10-depleted cells undergoing mitotic DNA synthesis (MIDAS; Fig. 2, A, I, and J; and Fig. S1 N), a process that resolves under-replicated DNA at CFSs in early mitosis (Minocherhomji et al., 2015). We conclude that ETAA1 is important for preventing mitotic chromosome abnormalities arising from incompletely replicated loci.

### Cell cycle- and replication stress-regulated phosphorylation of the ETAA1 AAD promotes its ATR-activating potential

In line with a role for ETAA1 in protecting against chromosome instability arising from under-replicated DNA even during unperturbed cell proliferation, previous work by others and us demonstrated that ETAA1 promotes ATR signaling in a normal S phase (Haahr et al., 2016; Saldivar et al., 2018). Because ETAA1 harbors both RPA-binding and ATR-activating determinants and might therefore be capable of promoting ATR activation irrespective of cell cycle position, we reasoned that regulatory control of this function may be important for its integration with

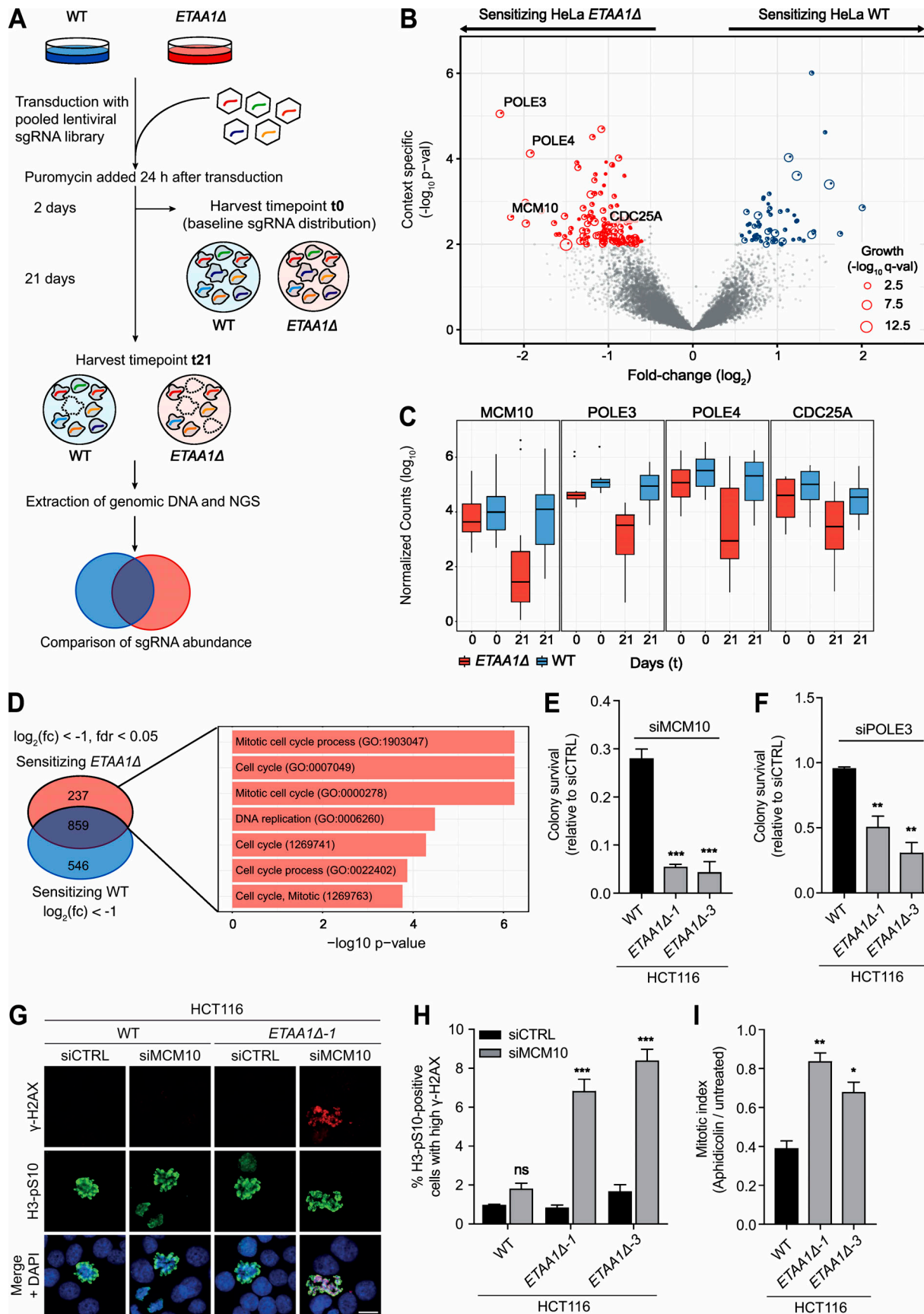


**Figure 1. ETAA1 becomes critical for cell fitness upon disruption of the DNA replication machinery.** (A) Schematic overview of CRISPR-Cas9 KO screen workflow. (B) Volcano plot of CRISPR-Cas9 screen results, showing gene KOs that selectively impair fitness of HeLa WT (blue;  $P < 0.01$ ) or *ETAA1Δ* (red;  $P < 0.01$ ) cells. Point sizes (q value) represent the corrected P value for growth effect ( $-\log_{10}$ ). Fold change depicts the median difference in sgRNA representation between the two cell lines at t21. (C) Boxplot depicting normalized counts for selected screen hits. (D) Gene ontology (GO) analysis of sensitizing hits specific to HeLa *ETAA1Δ* cells. (E) Clonogenic survival (relative to nontargeting control siRNA [siCTRL]) of HCT116 cell lines transfected with MCM10 siRNA (mean  $\pm$  SEM;  $n = 3$  independent experiments; unpaired *t* test). (F) As in E, but using POLE3 siRNA (mean  $\pm$  SEM;  $n = 3$  independent experiments; unpaired *t* test). (G) Representative images of siRNA-transfected cells coimmunostained with  $\gamma$ -H2AX and H3-pS10 antibodies. Scale bar, 10  $\mu$ m. (H) Flow cytometry analysis of  $\gamma$ -H2AX positivity in mitotic cells in G, gated based on DNA content and H3-pS10 positivity (mean  $\pm$  SEM;  $n = 3$  or 4 independent experiments; multiple *t* test). (I) Cells synchronized by double thymidine block were released into medium containing nocodazole in the presence or absence of APH (0.2  $\mu$ M), collected 12 h later, and processed for flow cytometry to determine the relative mitotic index (APH/untreated) by H3-pS10 staining (mean  $\pm$  SEM;  $n = 3$  experiments; unpaired *t* test). \*\*\*,  $P < 0.0005$ ; \*\*,  $P < 0.005$ ; \*,  $P < 0.05$ ; ns, not significant.

genome duplication status. The ATR-activating ability of TopBP1 can be stimulated by direct ATM-mediated phosphorylation within its AAD (Yoo et al., 2007). Correspondingly, we noted that the ETAA1 AAD contains highly conserved, putative CDK phosphorylation sites (S95 and S111 in human ETAA1) in close proximity to aromatic amino acids (F106 and W107) that are essential for stimulation of ATR kinase activity (Fig. 3 A; Bass et al., 2016; Haahr et al., 2016). Phospho-specific antibodies to S95 and S111 in human ETAA1 showed that both residues are phosphorylated in cells (Fig. 3, B and C; and Fig. S2 A). Interestingly, whereas the levels of S95 and S111 phosphorylation were low in asynchronous cells, these modifications were robustly up-regulated during S and G2 phases but declined as cells entered mitosis (Fig. 3 C). Using an established high-content imaging-based assay for monitoring ETAA1 AAD-mediated ATR activation in cells (Haahr et al., 2016; Thada and Cortez, 2019), we found that phospho-mimicking substitutions at S95 or S111 (S95D or S111D) but not other potential CDK sites within the ETAA1 AAD (T79D and T165D) potentiated the ATR-activating capacity of ectopic ETAA1 AAD expressed at low levels (Fig. 3 D and Fig. S2 B). Combining the S95D and S111D substitutions synergistically augmented this activity (Fig. 3 D and Fig. S2 B). Moreover, unlike WT ETAA1, whose AAD we have previously shown is a direct target of ATR-mediated phosphorylation (Haahr et al., 2016), an S95A+S111A AAD phosphorylation-deficient ETAA1 allele was refractory to phosphorylation by ATR upon replication stress (Fig. 3 E and Fig. S2, A and C). These observations suggested that phosphorylation of the ETAA1 AAD stimulates its ATR-activating potential and interplay with ATR. Interestingly, phosphorylation of S95 was strongly up-regulated upon replication stress induced by camptothecin or HU (Fig. 3 F and Fig. S2 D) in an ATR-dependent manner (Fig. 3 G and Fig. S2, E and F), while S111 phosphorylation showed a mild increase, indicating a potential positive feedback loop underlying ETAA1-mediated ATR activation.

Next, we investigated whether S95 and S111 were phosphorylated by CDKs. In contrast to ATR inhibition, suppressing interphase, but not mitotic, CDK activity strongly reduced the basal cell cycle-dependent phosphorylation of S95 and S111, but had no impact on the replication stress-induced hyperphosphorylation of S95 (Fig. 3 H and Fig. S2, F and G). Moreover, both S95 and S111 could be directly phosphorylated by cyclin A-CDK2, but not ATR, *in vitro* (Fig. S2, H and I). Collectively, these findings suggest that phosphorylation of S95 and S111 during unperturbed S phase is directly catalyzed by CDKs,

while replication stress-induced hyperphosphorylation of S95 is mediated by an ATR-dependent pathway involving an as yet unknown non-CDK effector kinase.

### AAD phosphorylation is critical for ETAA1-dependent suppression of replication stress-induced chromosome instability

We next asked whether the ETAA1 AAD and its phospho-dependent regulation are required for suppressing chromosome instability following impaired DNA replication progression, using a panel of ETAA1 KO cell lines stably reconstituted with inducible WT or mutant forms of GFP-tagged ETAA1 (Fig. S3 A). As expected, the mitotic chromosome abnormalities and increased MiDAS resulting from ETAA1 loss could be rescued by ectopic WT ETAA1, but not mutants lacking the AAD or RPA-binding motifs (Fig. 4, A–E; and Fig. S3 B), providing a framework for probing the importance of ETAA1 AAD phosphorylation in protecting against chromosomal aberrations. Notably, similar to the ETAA1  $\Delta$ AD and  $\Delta$ RPA1+2 mutants, the ETAA1 S95A+S111A mutant failed to efficiently reverse mitotic chromosome aberrations and DNA synthesis in an *ETAA1Δ* background, supporting a key role for AAD phosphorylation in promoting ETAA1-mediated suppression of chromosome instability (Fig. 4, D–H; and Fig. S3 C). We previously demonstrated that ETAA1 promotes cell survival following replication stress in a manner dependent on both its AAD and dual RPA-binding motifs (Haahr et al., 2016). Similarly, we found that stably reconstituted ETAA1 S95A+S111A protein was unable to correct the survival defect of *ETAA1Δ* cells exposed to replication stress (Fig. 4 I). These data further support an important role of phosphorylation-mediated regulation of ATR activation by ETAA1 in promoting genome stability and cell fitness when DNA replication integrity is challenged.

Our studies demonstrate that ETAA1 becomes critical for chromosome stability and cell fitness under conditions of compromised DNA replication efficiency, and that phosphorylation-mediated control of its ATR-stimulating potential is central to this function. The notion that ETAA1 suppresses a range of mitotic chromosome abnormalities associated with incompletely replicated DNA via its ATR-activating ability is well aligned with recent work by others and us showing that ETAA1, but not TopBP1, promotes ATR signaling during a normal S phase (Haahr et al., 2016; Saldivar et al., 2018). Moreover, in contrast to ETAA1, TopBP1 has been shown to localize to UFBs and promote MiDAS (Pedersen et al., 2015). This apparent division of

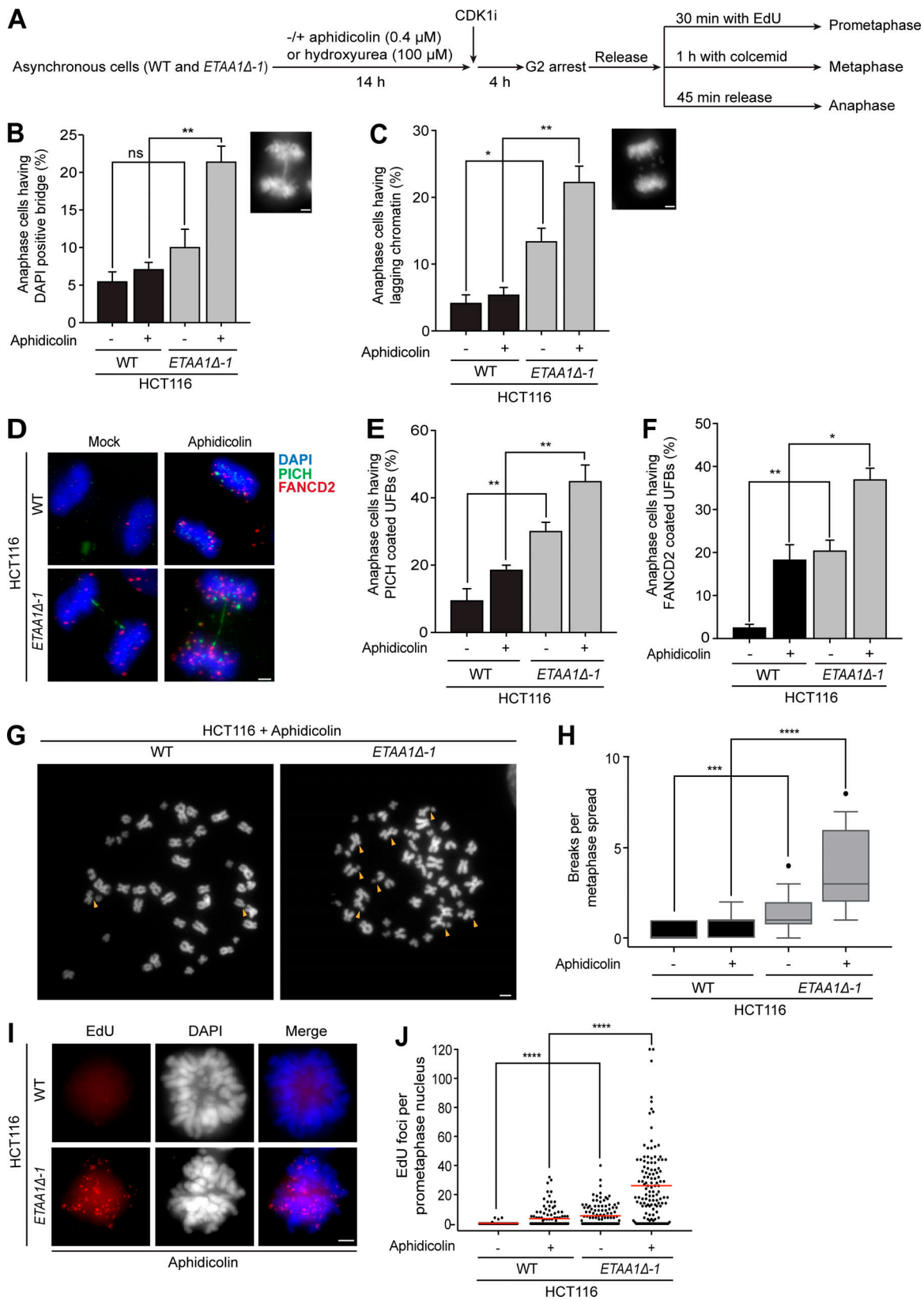


Figure 2. **ETAA1 suppresses mitotic chromosome abnormalities associated with incompletely replicated DNA.** (A) Workflow for analysis of mitotic chromosome abnormalities. (B) Quantification of DAPI-positive chromatin bridges (example shown in inset) in anaphase HCT116 cells treated as in A (mean  $\pm$  SEM;  $n = 3$  independent experiments; 100 anaphases/condition; unpaired  $t$  test). (C) As in B, except that the proportion of cells with lagging chromatin (inset) was quantified (mean  $\pm$  SEM;  $n = 3$  independent experiments; 100 anaphases/condition; unpaired  $t$  test). (D) Representative images of PICH-coated UFBs in anaphase HCT116 cells treated as in A and coimmunostained with PICH and FANCD2 antibodies. FANCD2 foci at UFB termini demarcating CFSs can be seen.

**(E and F)** Quantification of data in D (mean  $\pm$  SEM;  $n = 3$  independent experiments; 120 anaphases/condition; unpaired *t* test). **(G)** Representative images showing breaks (indicated by arrows) on metaphase chromosomes from APH-exposed HCT116 cells treated as in A. **(H)** Quantification of data in G. Box plot shows the median, upper and lower quartiles (boxes), and 10th and 90th percentiles (whiskers; 25–35 metaphases/condition; Kruskal–Wallis test). **(I)** Representative images of EdU incorporation in prometaphase nuclei demarcating MiDAS in HCT116 cells treated as in A. **(J)** Quantification of data in I (red bars, median;  $n = 3$  independent experiments; 120–130 prometaphases/per condition; Kruskal–Wallis test). \*\*\*\*,  $P < 0.0001$ ; \*\*\*,  $P < 0.0005$ ; \*\*,  $P < 0.005$ ; \*,  $P < 0.05$ ; ns, not significant. Scale bars, 2  $\mu$ m.

labor between ETAA1 and TopBP1 has a notable analogy to the distinct roles played by AAD-containing proteins in budding yeast, where Dna2 promotes activation of the ATR homologue Mec1 at RPA-coated single-stranded DNA on the lagging strand during normal DNA replication, whereas the TopBP1 homologue, Dpb11, drives Mec1-Rad53 activation upon replication stress (Bastos de Oliveira et al., 2015). We established that cell cycle- and replication stress-responsive phosphorylation of residues within the AAD core are critical for integrating the ATR-activating potential of ETAA1 with DNA replication status and for its ability to suppress chromosome instability. Recent insights into the structure of Mec1-Ddc2, the yeast homologue of ATR-ATRIP, suggested that acidic patches within AADs may interact with the basic C-terminal PRD (PIKK regulatory domain) domain in Mec1/ATR to promote conformational changes associated with kinase activation (Wang et al., 2017). This offers a possible mechanistic rationale for how negatively charged, phosphorylated residues within the ETAA1 AAD domain might enhance its ATR-activating potential, a notion awaiting validation by biochemical or structural approaches.

While an intra-mitotic function of ETAA1 was recently reported (Bass and Cortez, 2019), the role of ETAA1 in suppressing mitotic chromosome aberrations described here seems unlikely to reflect such an involvement for three reasons. First, the spectrum of mitotic chromosome abnormalities accumulating in *ETAA1Δ* cells exposed to mild replication stress is characteristic of defects arising due to the persistence of unresolved replication intermediates (Mankouri et al., 2013). Second, the stimulatory phosphorylations within the ETAA1 AAD, which we show are important for its ability to suppress chromosome abnormalities associated with under-replicated DNA, are largely confined to S/G2-phase cells and present at only low levels in mitosis. Third, we did not observe significant defects in Aurora B-associated mitotic phosphorylation events in our *ETAA1Δ* cell lines (Fig. S3, D and E).

Collectively, our data suggest that whereas TopBP1 may be the principal activator of the essential ATR-CHK1 checkpoint pathway, the role of ETAA1 in promoting cell fitness becomes particularly important following impediments to the DNA replication machinery that increase the risk posed by mitotic entry in the presence of unresolved DNA replication intermediates. This could help to explain why ETAA1 deficiency in mice manifests with partially penetrant lethality during embryogenesis and defective clonal expansion of T lymphocytes (Miosge et al., 2017), processes entailing rapid cell proliferation where efficient ETAA1-mediated G2/M checkpoint control may be instrumental in suppressing gross chromosomal instability. Targeted inhibition of ETAA1 functionality might thus unmask a selective

vulnerability in highly proliferative malignant cells that generally experience deregulated control of cell cycle progression and elevated replicative stress, providing potential opportunities for the continued evolution of promising therapeutic strategies targeting ATR signaling in cancer (Lecona and Fernandez-Capetillo, 2018).

## Materials and methods

### Cell culture

Human U2OS, HCT116, HeLa, and HEK293FT cell lines obtained from American Type Culture Collection were cultured in DMEM containing 10% FBS and regularly tested negative for mycoplasma infection. HeLa and HCT116 cell lines with targeted KO of ETAA1 (*ETAA1Δ*), generated by transfecting parental cells with pX459-sgETAA1 construct and selected with puromycin, were described previously (Haahr et al., 2016). To generate derivative cell lines inducibly expressing WT or mutant forms (S95A+S111A,  $\Delta$ RBM1+2 [ $\Delta$ 603-618+ $\Delta$ 892-926], and  $\Delta$ AAD [ $\Delta$ 56-220]) of GFP-tagged human ETAA1, HCT116 *ETAA1Δ* cells were cotransfected with pcDNA4/TO-GFP-ETAA1 and pcDNA6/TR (Invitrogen) plasmids, and positive clones were selected by incubation in medium containing Blasticidin S (Invitrogen) and Zeocin (Invitrogen) for 14 d.

Unless otherwise stated, the following drug concentrations were used: thymidine (2 mM; Sigma-Aldrich), camptothecin (1  $\mu$ M; Sigma-Aldrich), HU (2 mM; Sigma-Aldrich), ATR inhibitor (AZ20; 1  $\mu$ M; Sigma-Aldrich), APH (0.4  $\mu$ M; Sigma-Aldrich), pan-CDK inhibitor (R547; 5  $\mu$ M; Sigma-Aldrich), CDK1 inhibitor (RO-3306; 7  $\mu$ M; Millipore), nocodazole (40 ng/ml), and colcemid (0.1  $\mu$ g/ml).

### Plasmids and siRNA

For doxycycline-inducible expression of GFP-ETAA1, cDNA encoding human ETAA1 was cloned into the destination vector pcDNA4/TO-GFP using Gateway LR Clonase (Invitrogen). For nuclear expression of the ETAA1 AAD, cDNA encoding residues 56–220 of human ETAA1 was inserted between the GFP and 3xNLS (nuclear localization signal) tags in the pAcGFP-Nuc vector (Clontech), as described previously (Haahr et al., 2016). To ensure optimal fluorescence detection, ETAA1 AAD(56–220)-3xNLS was subcloned into pEGFP-C1 (Clontech). Introduction of point mutations into pcDNA4/TO-GFP-ETAA1 (S95A+S111A) and pEGFP-C1-ETAA1-AAD-3xNLS (FW/AA [F106A+W107A], S95D, S111D, S95D+S111D, T79D, and T165D) was performed using a Q5 Site-directed mutagenesis kit (NEB), according to the manufacturer's protocol.

Plasmid DNA transfections were performed with FuGENE 6 (Promega) or GeneJuice (Merck Millipore), according to the

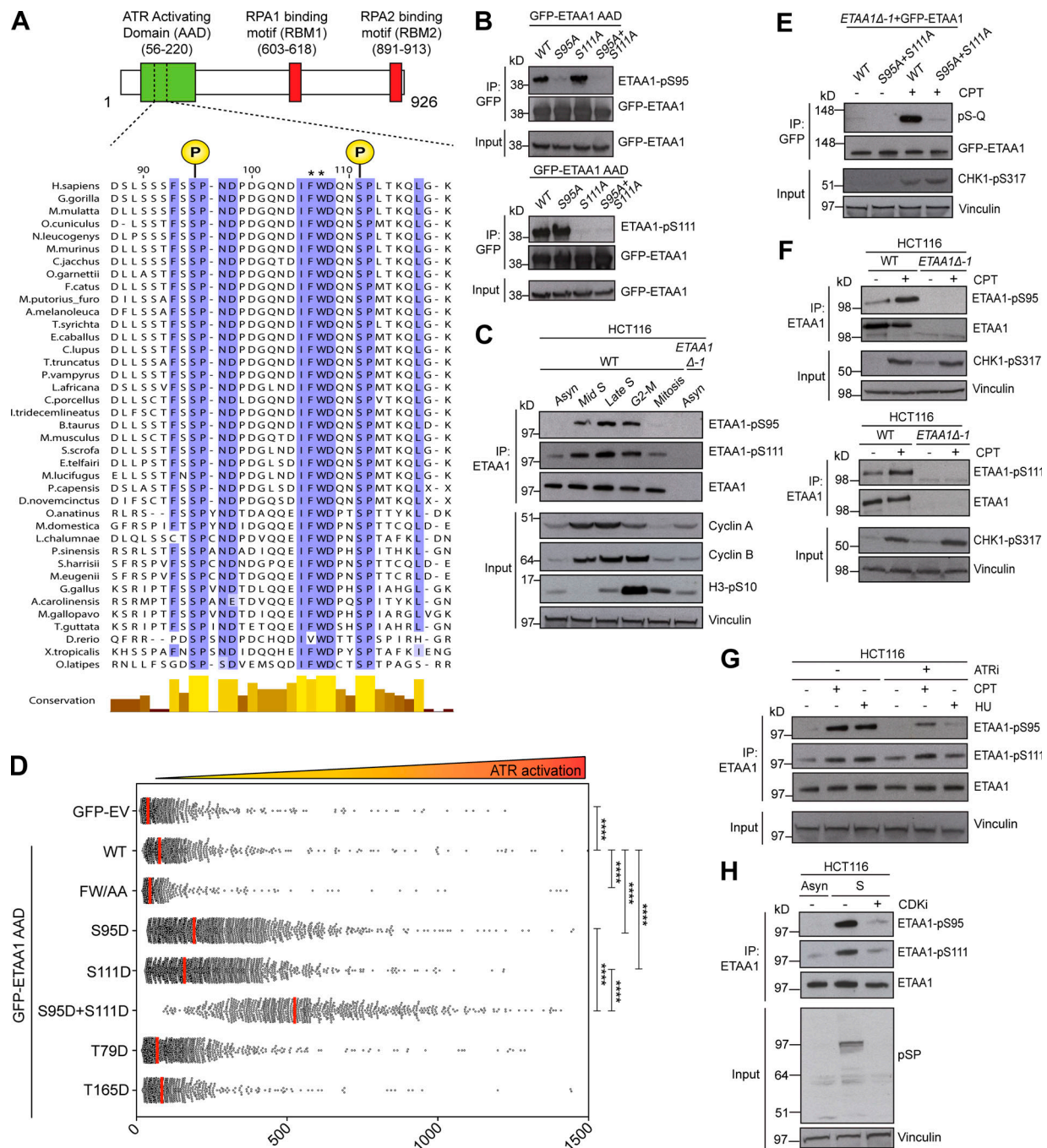


**Figure 3. Cell cycle- and replication stress-regulated phosphorylation of the ETAA1 AAD promotes its ATR-activating potential.** (A) Sequence alignment of the ETAA1 AAD core region. Highly conserved residues (blue) and aromatic residues required for ATR activation (asterisks) are indicated. (B) Extracts of HCT116 cells transfected with WT or mutant versions of GFP-ETAA1 AAD were subjected to GFP IP under denaturing conditions and immunoblotting (IB). (C) Cells released from a G1/S arrest by double thymidine block and collected 4 h (mid-S phase), 8 h (late S), 12 h (G2-M), or 21 h (prometaphase arrested with nocodazole) later were processed for IP of endogenous ETAA1 under denaturing conditions followed by IB. (D) U2OS cells transfected with GFP-ETAA1 AAD-3xNLS constructs were immunostained with  $\gamma$ -H2AX antibody and analyzed by quantitative imaging to reveal single-cell correlations between GFP expression and pan-nuclear  $\gamma$ -H2AX signal intensity as readout for ETAA1-induced ATR activation (Haahr et al., 2016; Thada and Cortez, 2019). Plot shows mean  $\gamma$ -H2AX signal intensity in cells expressing GFP-ETAA1 AAD-3xNLS at a low level (Fig. S2 B) from a representative experiment (red bars, median; \*\*\*\*,  $P < 0.0001$ , Kruskal-Wallis test; >800 cells quantified per condition). (E) HCT116 *ETAA1Δ* cells stably expressing GFP-ETAA1 WT or S95A+S111A mutant were exposed or not to CPT for 90 min and subjected to GFP IP under denaturing conditions followed by IB. (F) Cells were exposed or not to CPT for 90 min and processed as in C. (G) Cells incubated with CPT or HU for 90 min in the presence or absence of ATR inhibitor (ATRi) were processed as in F. (H) As in C, except that cells in late S phase (S) were treated or not with CDK inhibitor (CDKi) for 90 min before harvesting. Asyn, asynchronous cells.

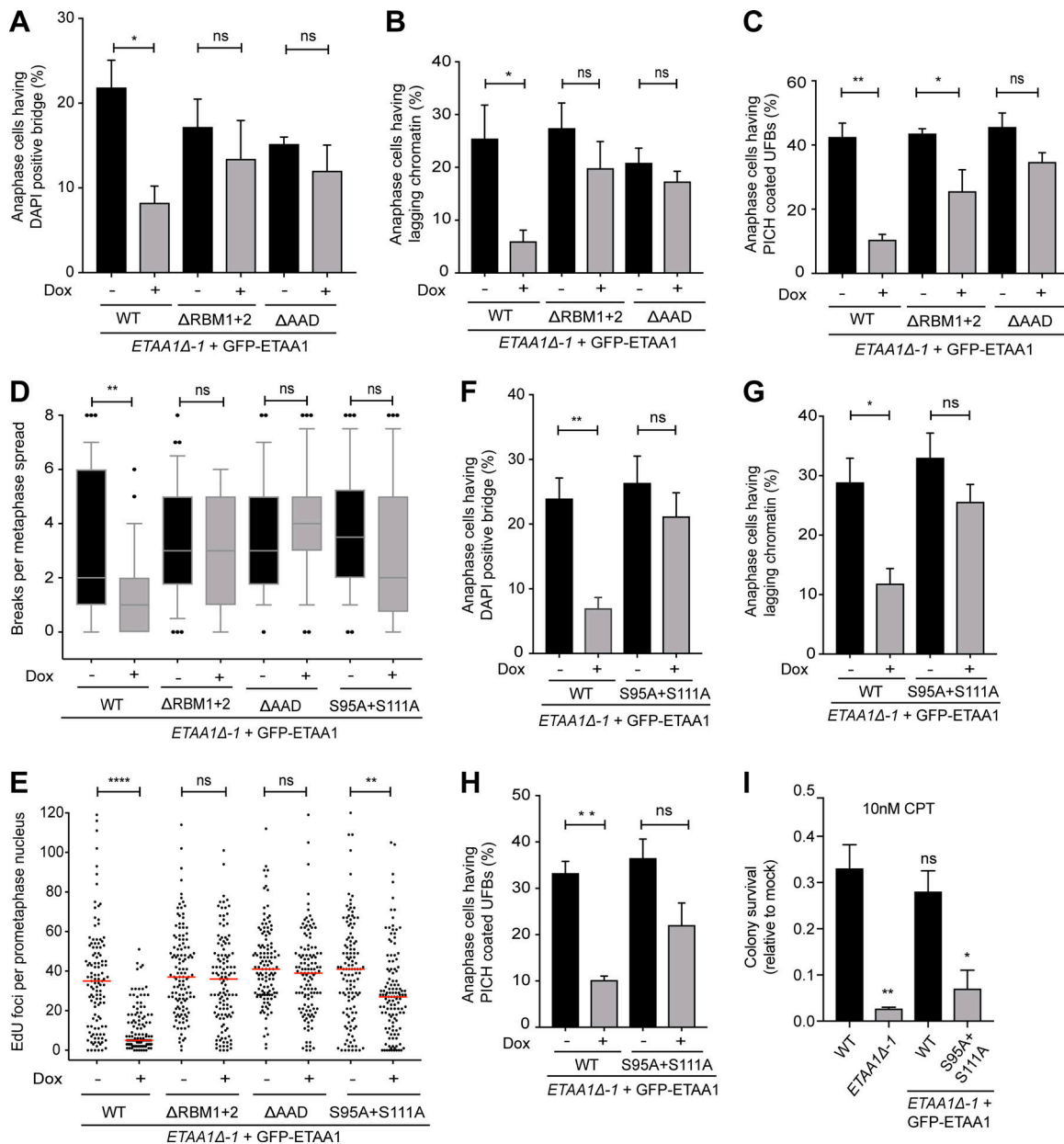


**Figure 4. Phospho-dependent regulation of ETAA1-mediated ATR activation promotes chromosome stability.** (A) HCT116 *ETAA1Δ* cells stably reconstituted with GFP-ETAA1 WT or mutant alleles were grown in the presence of doxycycline (Dox) to express the transgenes or kept uninduced (Fig. S3 A), then subjected to low-dose APH treatment before synchronization in G2 and release into mitosis as in Fig. 2 A. DAPI-positive chromatin bridges were quantified (mean ± SEM; *n* = 3 independent experiments; 120 anaphases/condition; unpaired *t* test). (B) Lagging chromatin in cells in A (mean ± SEM; *n* = 3 independent experiments; 120 anaphases/condition; unpaired *t* test). (C) Cells in A were immunostained with PICH antibody and analyzed for PICH-coated UFBs (mean ± SEM; *n* = 3 independent experiments; 150 anaphases/condition; unpaired *t* test). (D) Chromosome breaks in metaphase spreads of cells treated as in A were scored. Box plot shows median, upper and lower quartiles (boxes), and 10th and 90th percentiles (whiskers; 40 metaphases/condition; Kruskal–Wallis test). (E) As in D, but EdU foci in prometaphase were quantified (red bars, median; 120–125 prometaphases/condition; Kruskal–Wallis test). (F) As in A, using indicated cell lines (mean ± SEM; *n* = 3 independent experiments; 120 anaphases/condition; unpaired *t* test). (G) Lagging chromatin in cells in F (mean ± SEM; *n* = 3 independent experiments; 120 anaphases/condition; unpaired *t* test). (H) As in C, using indicated cell lines (mean ± SEM; *n* = 3 independent experiments; 150 anaphases/condition; unpaired *t* test). (I) Clonogenic survival of CPT-treated HCT116 WT and *ETAA1Δ* cell lines stably expressing GFP-ETAA1 WT or S95A+S111A mutant. Results were normalized to mock treatment (mean ± SEM; *n* = 3 independent experiments; unpaired *t* test). \*\*\*\*, *P* < 0.0001; \*\*, *P* < 0.005; \*, *P* < 0.05; ns, not significant.

manufacturer’s instructions. For siRNA transfections (typically 48–72 h), Lipofectamine RNAiMAX (Invitrogen) was used according to the manufacturer’s protocol. All siRNAs were used at a final concentration of 50 nM. The following siRNA

oligonucleotides were used: non-targeting control: 5’-GGGAUACCUAGACGUUCUA-3’; MCM10, 5’-GACGAUUCUGGAACAA A-3’; and POLE3, ON-TARGET Plus POLE3 siRNA pool (LQ-008460-01-0002; Dharmacon; Bellelli et al., 2018).



### Genome-scale CRISPR-Cas9 screen

For preparation of lentivirus, HEK293FT cells were transfected with a human CRISPR KO pooled library (GeCKO v2; 1000000048; Addgene) and the lentiviral packaging plasmids pMDLg/pRRE, pRS-Rev, and pMD2.G using Lipofectamine 3000 according to the manufacturer's protocol. After 3 d, the supernatant was passed through a 0.45- $\mu$ m syringe filter unit, and the multiplicity of infection was determined. HeLa WT and *ETAA1 $\Delta$*  cells were infected with the pooled lentiviral library at a multiplicity of infection of 0.3 and selected with puromycin 24 h after transduction. After 2 d of puromycin selection, a fraction of the cells was harvested ("t0" time point), and the remaining cells were cultured for 21 d ("t21" time point). The experiment was performed in duplicates, and library coverage was kept at a minimum of 200 $\times$  per replicate throughout the entire screen. Genomic DNA was extracted from  $3 \times 10^7$  cells as described previously (Chen et al., 2015).

From 130  $\mu$ g genomic DNA, sgRNA sequences were amplified by PCR using Herculase II Fusion DNA polymerase kit with the following primers: CRISPR F1, 5'-AATGGACTATCATATGCTTACCGTAACTTGAAAGTATTTTCG-3', and CRISPR R1, 5'-TCTACTATTCTTCCCTGCACTGTTGTGGCGCATGTGCGCTCTG-3'. A second PCR was then performed to attach Illumina adaptors and barcodes with primer sequences described previously (Shalem et al., 2014).

The amplicons from the second PCR were gel-extracted and subjected to next-generation DNA sequencing. Samples from WT and *ETAA1 $\Delta$*  cells were multiplexed and subjected to single-end 75-bp-read high-throughput DNA sequencing on an Illumina NextSeq instrument with 30% PhiX spike-in, generating more than 400 million reads. Analysis of sgRNA count data was conducted using MEMcrispR (<https://github.com/grimbough/MEMcrispR>). MEMcrispR uses linear mixed-effect models for each gene to assess the fold change and significance between two conditions. The use of mixed effect allows addition of "fixed" and "random" terms to the model. Days of cell growth (t0 and t21) and the cell lines correspond to "fixed" effects, whereas the sgRNAs and the replicates correspond to "random" effects. The data were normalized by the median distribution of the internal nontargeting sgRNAs. Two models were calculated, one with the treatment effect (t0 versus t21) and a null model without treatment. An ANOVA likelihood ratio test was calculated between the two models to estimate significant differences. The data were corrected for multiple testing using the Benjamini-Hochberg procedure. The  $\beta$  scores were converted to fold changes and used for the directionality of the effect of each gene (positive or negative) as well as for the magnitude of the effect. Fold changes represent sgRNA read counts between treatment and control conditions. MEMcrispR identifies differentially represented genes between t0 versus t21 and combined, and the advanced models use the cell line as an additional fixed parameter. Data from MEMcrispR analysis using the cell line effect are shown, and hits are specific to HeLa *ETAA1 $\Delta$*  or WT cells (q values for growth are depicted). Gene ontology enrichment analysis was performed on the individual analyses of each cell line. Terms were calculated by ToppGene and reduced by Revigo.

### Immunoblotting, immunoprecipitation (IP), and dot blot analysis

For immunoblotting experiments, cells were lysed in EBC buffer (50 mM Tris-HCl, pH 7.5, 150 mM NaCl, 1 mM EDTA, 0.5% NP-40, and 1 mM DTT) containing protease and phosphatase inhibitors and sonicated, and the lysate was clarified by centrifugation. For IP of endogenous ETAA1, cells were lysed in denaturing buffer (20 mM Tris-HCl, pH 7.5, 50 mM NaCl, 1 mM EDTA, 0.5% Igepal, 0.5% sodium deoxycholate, and 0.5% SDS) supplemented with protease and phosphatase inhibitors. Cleared lysates were incubated with ETAA1 antibody (1.5–2  $\mu$ g/sample) coupled to Protein G agarose beads (20398; Thermo Fisher Scientific) overnight at 4°C on a rotary wheel. Beads with bound proteins were washed four times with denaturing buffer and eluted by boiling in 2 $\times$  Laemmli sample buffer. GFP IPs were performed using similar conditions, except that cell lysates were incubated with GFP-Trap agarose (Chromotek) for 3 h at 4°C with rotation. For dot blots, N-terminally biotin-labeled unmodified or S95-/S111-phosphorylated peptides spanning amino acids 91–115 of human ETAA1 (SSFSSPNDPDGQNDIFWDQNSPLTK and SSFS(pS)PNDPDGQNDIFWDQN(pS)PLTK; synthesized by Peptide 2.0) were spotted onto a 0.22- $\mu$ m nitrocellulose membrane (Whatman Protran BA83). The membrane was dried for 30 min and processed for immunoblotting.

Antibodies used in this study included mouse monoclonals to actin (MAB1501; Millipore), cyclin A (611268; BD Biosciences), cyclin B (610220; BD Biosciences), GFP (11814460001; Roche),  $\gamma$ -H2AX (2577, Cell Signaling; and 05-636, Millipore), PICH (04-1540; Millipore), and vinculin (V9131; Sigma-Aldrich); rabbit polyclonals to Aurora B pT232 (600-401-677; Rockland), Chk1 pS317 (2344; Cell Signaling), FANCD2 (NB100-182; Novus Biologicals), GFP (sc-8334; Santa Cruz), histone H3-pS10 (06-570; Millipore), MCM10 (12251-1-AP; Proteintech Europe), phospho-(Ser) CDK substrate (pSP; 2324; Cell Signaling), and phospho-ATM/ATR substrate (pSQ; 9607; Cell Signaling). Polyclonal phospho-specific antibodies to S95 and S111 in human ETAA1 were produced in rabbit (GenScript) using internal ETAA1 peptides as antigens. Polyclonal sheep ETAA1 antibody raised against full-length human ETAA1 was described previously (Haahr et al., 2016).

### Immunofluorescence microscopy

Cells were washed twice in PBS before fixation with 4% formaldehyde for 15 min. Cells were then subjected to a permeabilization step with PBS containing 0.2% Triton X-100 for 5 min and incubated with primary antibodies diluted in PBS containing 2% BSA for 1 h at room temperature. Following incubation with secondary antibodies (Alexa Fluor; Life Technologies) diluted in PBS containing 2% BSA for 1 h at room temperature, coverslips were mounted in Vectashield mounting medium (Vector Laboratories) containing DAPI nuclear stain (Molecular Probes). Images were acquired with a Leica AF6000 wide-field microscope (Leica Microsystems) equipped with HC Plan-Apochromat 63 $\times$ /1.4 oil immersion objective, using standard settings. Image acquisition and analysis were performed with LAS X software (Leica Microsystems). Raw images were exported as TIFF files, and if adjustments in image contrast

and brightness were applied, identical settings were used on all images of a given experiment.

For high-content imaging and analysis of EGFP-ETAA1-AAD-3xNLS expression, cells were fixed, permeabilized, and stained as described above. Nuclear DNA was counterstained with DAPI alongside incubation with secondary antibodies. Cells were then mounted onto glass slides using ProLong Gold Antifade (Invitrogen, Molecular Probes). Images were acquired with an Olympus IX-81 wide-field microscope equipped with an MT20 Illumination system and a digital monochrome Hamamatsu C9100 CCD camera. Olympus UPLSAPO 10×/0.4 NA and 20×/0.75 NA objectives were used. Automated and unbiased image analysis was performed with the ScanR analysis software. Data were exported and processed using Spotfire (Tibco) software.

### Analysis of mitotic chromosome abnormalities

Asynchronously growing cells were mock-treated or incubated with APH (0.4 μM) or HU (100 μM) for 14 h, and subsequently treated with the CDK1 inhibitor (CDK1i) RO-3306 (7 μM) for 4 h. For analysis of chromatin bridges, lagging chromatin, and UFBs, G2-arrested cells were washed and released into fresh pre-warmed medium for 45 min. Cells were fixed with 4% paraformaldehyde containing 0.2% Triton X-100 in PBS for 20 min. For MiDAS analysis, G2-arrested cells were released into fresh medium containing EdU (20 μM) for 30 min. Prometaphase cells were gently shaken off and spotted on poly-L-lysine slides. Cells were fixed with 4% paraformaldehyde, and the Click-iT reaction was performed as described previously (Minocherhomji et al., 2015). For metaphase spreads, G2-arrested cells were released into fresh medium containing colcemid (0.1 μg/ml) for 1 h. Mitotic cells were shaken off, treated with hypotonic buffer (35 mM KCl) for 15 min, resuspended in methanol/acetic acid (3:1) solution, and spread onto glass slides.

### Flow cytometry

Cells collected by trypsinization were fixed in 70% ethanol, permeabilized in 0.25% Triton X-100 for 10 min, and washed in PBS containing 2% BSA. Cells were incubated with primary antibodies diluted in PBS containing 2% BSA for 1 h at room temperature, followed by a washing step in PBS containing 2% BSA. Cells were then stained for 1 h with secondary antibody (Alexa Fluor; Life Technologies) and washed, and DNA was counterstained in PBS containing 0.1 mg/ml propidium iodide containing RNase (19101; 20 μg/ml; Qiagen) for 30 min at 37°C or, alternatively, with DAPI. Flow cytometry analysis was performed using a FACS Calibur (BD Biosciences) and CellQuest Pro software, or using a LSR Fortessa (BD Biosciences) and FACSDiva software. Exported data were analyzed using FlowJo software (v.10.1).

### Clonogenic survival assays

For colony formation assays, cells were counted and, where indicated, reverse-transfected with siRNAs for 48 h. Cells were then seeded in dishes in triplicates and incubated for 7–10 d to form visible colonies. To assay camptothecin (CPT) sensitivity, cells were allowed to adhere for a minimum of 16 h following seeding and then treated with 10 nM CPT for 24 h, washed, and

released into fresh medium. After 7–10 d of colony outgrowth, plates were washed once in PBS, left to dry, and stained with cell staining solution (0.5% wt/vol Crystal Violet; 25% vol/vol methanol). Colonies were counted using an automated colony counter and its associated software (GelCount; Oxford Op-tronix). The surviving fraction was calculated as no. colonies/(no. seeded cells × plating efficiency) and normalized to mock control.

### In vitro kinase assays

GST-tagged ETAA1(56–220) was expressed in Rosetta 2 (DE3) pLysS bacteria and purified using glutathione-based affinity purification. For radioactive kinase assays, 100 ng of purified His-Cyclin A/CDK2 (PV3267; Thermo Fisher Scientific) was incubated with 2 μg recombinant GST-ETAA1(56–220) in kinase assay buffer (10 mM MnCl<sub>2</sub>, 1 mM DTT, and 50 mM β-glycerophosphate). Reactions were started by addition of 100 μM ATP spiked with [γ-<sup>32</sup>P]ATP (1 μCi; Perkin Elmer), incubated at 30°C with gentle shaking, and terminated by addition of Laemmli sample buffer and boiling for 10 min. Samples were then resolved by SDS-PAGE and stained with Colloidal Blue (Life Technologies). Relative phosphorylation was assayed by autoradiography. For kinase assays comparing cyclin A/CDK2 and ATR/ATRIP kinase activity toward the ETAA1 AAD, 100 ng of purified His-cyclin A/CDK2 or FLAG-ATR/Myc-ATRIP (14–953; Eurofins) was incubated with 2 μg recombinant GST-ETAA1(56–220) and kinase assay buffer. Samples were processed as above and immunoblotted with phospho-specific antibodies to ETAA1 S95 and S111.

### Quantification and statistical analysis

Statistical analysis of data was performed using GraphPad Prism (version 7). Information about statistical tests is provided in the figure legends. No samples were excluded from the analysis, and no statistical method was used to predetermine sample size. For all experiments, samples were not randomized, and the investigators were not blinded to the group allocation during experiments and outcome assessment.

### Online supplemental material

Fig. S1 shows the impact of ETAA1 deficiency on clonogenic survival and mitotic chromosome abnormalities. Fig. S2 shows the characterization of ETAA1 S95 and S111 phosphorylation. Fig. S3 shows the impact of altered ETAA1 functional status on mitotic chromosome abnormalities and Aurora B-dependent phosphorylation events. Table S1 shows full results and analysis of genome-scale CRISPR-Cas9 KO screen in HeLa WT and ETAA1Δ cells.

### Acknowledgments

We thank Francisco G. Rodriguez Gonzalez for assistance with next-generation sequencing, and Michal Zimmermann and Daniel Durocher for technical advice on CRISPR screens.

This work was supported by the Novo Nordisk Foundation (grant no. NNF14CC0001), Independent Research Fund Denmark (grant no. 7016-00055), European Research Council (grant

agreement no. 616236 [DDRRegulation]), Danish National Research Foundation (grant no. DNR15), and Danish Cancer Society (grant no. A10769).

The authors declare no competing financial interests.

Author contributions: D. Achuthankutty, R.S. Thakur, P. Haahr, and S. Hoffmann carried out experiments. D. Achuthankutty, R.S. Thakur, P. Haahr, S. Hoffmann, A.P. Drainas, A.H. Bizard, J. Weischenfeldt, I.D. Hickson, and N. Mailand designed experiments and analyzed the data. N. Mailand wrote the manuscript, and all authors edited it.

Submitted: 9 May 2019

Revised: 28 August 2019

Accepted: 10 September 2019

## References

- Bartek, J., C. Lukas, and J. Lukas. 2004. Checking on DNA damage in S phase. *Nat. Rev. Mol. Cell Biol.* 5:792–804. <https://doi.org/10.1038/nrmi493>
- Bass, T.E., and D. Cortez. 2019. Quantitative phosphoproteomics reveals mitotic function of the ATR activator ETAA1. *J. Cell Biol.* 218:1235–1249.
- Bass, T.E., J.W. Luzwick, G. Kavanaugh, C. Carroll, H. Dugrawala, G.G. Glick, M.D. Feldkamp, R. Putney, W.J. Chazin, and D. Cortez. 2016. ETAA1 acts at stalled replication forks to maintain genome integrity. *Nat. Cell Biol.* 18:1185–1195. <https://doi.org/10.1038/ncb3415>
- Bastos de Oliveira, F.M., D. Kim, J.R. Cussiol, J. Das, M.C. Jeong, L. Doerfler, K.H. Schmidt, H. Yu, and M.B. Smolka. 2015. Phosphoproteomics reveals distinct modes of Mec1/ATR signaling during DNA replication. *Mol. Cell.* 57:1124–1132. <https://doi.org/10.1016/j.molcel.2015.01.043>
- Bellelli, R., V. Borel, C. Logan, J. Svendsen, D.E. Cox, E. Nye, K. Metcalfe, S.M. O'Connell, G. Stamp, H.R. Flynn, et al. 2018. Polepsilon Instability Drives Replication Stress, Abnormal Development, and Tumorigenesis. *Mol. Cell.* 70:707–721.
- Branzei, D., and M. Foiani. 2010. Maintaining genome stability at the replication fork. *Nat. Rev. Mol. Cell Biol.* 11:208–219. <https://doi.org/10.1038/nrm2852>
- Chadha, G.S., A. Gambus, P.J. Gillespie, and J.J. Blow. 2016. Xenopus Mcm10 is a CDK-substrate required for replication fork stability. *Cell Cycle.* 15: 2183–2195. <https://doi.org/10.1080/15384101.2016.1199305>
- Chan, Y.W., K. Fugger, and S.C. West. 2018. Unresolved recombination intermediates lead to ultra-fine anaphase bridges, chromosome breaks and aberrations. *Nat. Cell Biol.* 20:92–103. <https://doi.org/10.1038/s41556-017-0011-1>
- Chen, S., N.E. Sanjana, K. Zheng, O. Shalem, K. Lee, X. Shi, D.A. Scott, J. Song, J.Q. Pan, R. Weissleder, et al. 2015. Genome-wide CRISPR screen in a mouse model of tumor growth and metastasis. *Cell.* 160:1246–1260. <https://doi.org/10.1016/j.cell.2015.02.038>
- Ciccio, A., and S.J. Elledge. 2010. The DNA damage response: making it safe to play with knives. *Mol. Cell.* 40:179–204. <https://doi.org/10.1016/j.molcel.2010.09.019>
- Delacroix, S., J.M. Wagner, M. Kobayashi, K. Yamamoto, and L.M. Karnitz. 2007. The Rad9-Hus1-Rad1 (9-1-1) clamp activates checkpoint signaling via TopBP1. *Genes Dev.* 21:1472–1477. <https://doi.org/10.1101/gad.1547007>
- Haahr, P., S. Hoffmann, M.A. Tollenaere, T. Ho, L.I. Toledo, M. Mann, S. Bekker-Jensen, M. Räsche, and N. Mailand. 2016. Activation of the ATR kinase by the RPA-binding protein ETAA1. *Nat. Cell Biol.* 18:1196–1207. <https://doi.org/10.1038/ncb3422>
- Kabeche, L., H.D. Nguyen, R. Buisson, and L. Zou. 2018. A mitosis-specific and R loop-driven ATR pathway promotes faithful chromosome segregation. *Science.* 359:108–114. <https://doi.org/10.1126/science.aan6490>
- Kumagai, A., J. Lee, H.Y. Yoo, and W.G. Dunphy. 2006. TopBP1 activates the ATR-ATRIP complex. *Cell.* 124:943–955. <https://doi.org/10.1016/j.cell.2005.12.041>
- Lecona, E., and O. Fernandez-Capetillo. 2018. Targeting ATR in cancer. *Nat. Rev. Cancer.* 18:586–595. <https://doi.org/10.1038/s41568-018-0034-3>
- Lee, J., A. Kumagai, and W.G. Dunphy. 2007. The Rad9-Hus1-Rad1 checkpoint clamp regulates interaction of TopBP1 with ATR. *J. Biol. Chem.* 282: 28036–28044. <https://doi.org/10.1074/jbc.M704635200>
- Lee, Y.C., Q. Zhou, J. Chen, and J. Yuan. 2016. RPA-Binding Protein ETAA1 Is an ATR Activator Involved in DNA Replication Stress Response. *Curr. Biol.* 26:3257–3268. <https://doi.org/10.1016/j.cub.2016.10.030>
- Mankouri, H.W., D. Huttner, and I.D. Hickson. 2013. How unfinished business from S-phase affects mitosis and beyond. *EMBO J.* 32:2661–2671. <https://doi.org/10.1038/emboj.2013.211>
- Minocherhomji, S., S. Ying, V.A. Bjerregaard, S. Bursomanno, A. Aleliunaite, W. Wu, H.W. Mankouri, H. Shen, Y. Liu, and I.D. Hickson. 2015. Replication stress activates DNA repair synthesis in mitosis. *Nature.* 528: 286–290. <https://doi.org/10.1038/nature16139>
- Miosge, L.A., Y. Sontani, A. Chuah, K. Horikawa, T.A. Russell, Y. Mei, M.V. Wagle, D.R. Howard, A. Enders, D.C. Tschärke, et al. 2017. Systems-guided forward genetic screen reveals a critical role of the replication stress response protein ETAA1 in T cell clonal expansion. *Proc. Natl. Acad. Sci. USA.* 114:E5216–E5225.
- Pedersen, R.T., T. Kruse, J. Nilsson, V.H. Oestergaard, and M. Lisby. 2015. TopBP1 is required at mitosis to reduce transmission of DNA damage to G1 daughter cells. *J. Cell Biol.* 210:565–582. <https://doi.org/10.1083/jcb.201502107>
- Saldívar, J.C., D. Cortez, and K.A. Cimprich. 2017. The essential kinase ATR: ensuring faithful duplication of a challenging genome. *Nat. Rev. Mol. Cell Biol.* 18:622–636. <https://doi.org/10.1038/nrm.2017.67>
- Saldívar, J.C., S. Hamperl, M.J. Bocek, M. Chung, T.E. Bass, F. Cisneros-Soberanis, K. Samejima, L. Xie, J.R. Paulson, W.C. Earnshaw, et al. 2018. An intrinsic S/G<sub>2</sub> checkpoint enforced by ATR. *Science.* 361:806–810. <https://doi.org/10.1126/science.aap9346>
- Sanjana, N.E., O. Shalem, and F. Zhang. 2014. Improved vectors and genome-wide libraries for CRISPR screening. *Nat. Methods.* 11:783–784. <https://doi.org/10.1038/nmeth.3047>
- Shalem, O., N.E. Sanjana, E. Hartenian, X. Shi, D.A. Scott, T. Mikkelsen, D. Heckl, B.L. Ebert, D.E. Root, J.G. Doench, and F. Zhang. 2014. Genome-scale CRISPR-Cas9 knockout screening in human cells. *Science.* 343: 84–87. <https://doi.org/10.1126/science.1247005>
- Thada, V., and D. Cortez. 2019. Common motifs in ETAA1 and TOPBP1 required for ATR kinase activation. *J. Biol. Chem.* 294:8395–8402. <https://doi.org/10.1074/jbc.RA119.008154>
- Wang, X., T. Ran, X. Zhang, J. Xin, Z. Zhang, T. Wu, W. Wang, and G. Cai. 2017. 3.9 Å structure of the yeast Mec1-Ddc2 complex, a homolog of human ATR-ATRIP. *Science.* 358:1206–1209. <https://doi.org/10.1126/science.aan8414>
- Yoo, H.Y., A. Kumagai, A. Shevchenko, A. Shevchenko, and W.G. Dunphy. 2007. Ataxia-telangiectasia mutated (ATM)-dependent activation of ATR occurs through phosphorylation of TopBP1 by ATM. *J. Biol. Chem.* 282:17501–17506. <https://doi.org/10.1074/jbc.M701770200>
- Zeman, M.K., and K.A. Cimprich. 2014. Causes and consequences of replication stress. *Nat. Cell Biol.* 16:2–9. <https://doi.org/10.1038/ncb2897>
- Zhou, Z.W., C. Liu, T.L. Li, C. Bruhn, A. Krueger, W. Min, Z.Q. Wang, and A.M. Carr. 2013. An essential function for the ATR-activation-domain (AAD) of TopBP1 in mouse development and cellular senescence. *PLoS Genet.* 9:e1003702. <https://doi.org/10.1371/journal.pgen.1003702>
- Zou, L., and S.J. Elledge. 2003. Sensing DNA damage through ATRIP recognition of RPA-ssDNA complexes. *Science.* 300:1542–1548. <https://doi.org/10.1126/science.1083430>